

The Mid-Infrared Color-Luminosity Relation and the Local 12 μm Luminosity Function

Fan Fang, David L. Shupe, Cong Xu, Perry B. Hacking
Infrared Processing and Analysis Center, Jet Propulsion Laboratory, Caltech 100-22,
Pasadena, CA 91125

ABSTRACT

We have established a model to systematically estimate the contribution of the mid-infrared emission features between 3 μm and 11.6 μm to the IRAS in-band fluxes, using the results of ISO PHT-S observation of 16 galaxies by Lu et al. (1997). The model is used to estimate more properly the k -corrections for calculating the restframe 12 and 25 μm fluxes and luminosities of IRAS galaxies.

We have studied the 12-25 μm color-luminosity relation for a sample of galaxies selected at 25 μm . The color is found to correlate well with the 25 μm luminosity, the mid-infrared luminosity, and the ratio of far-infrared and the blue luminosities. The relations with the mid-infrared luminosities are more sensitive to different populations of galaxies, while a single relation of the 12-25 μm color vs. the ratio of the far-infrared and the blue luminosities applies equally well to these different populations. The luminous and ultraluminous infrared galaxies have redder 12-25 μm colors than those of the quasars. These relations provide powerful tools to differentiate different populations of galaxies.

The local luminosity function at 12 μm provides the basis for interpreting the results of deep mid-infrared surveys planned or in progress with ISO, WIRE and SIRTf. We have selected a sample of 668 galaxies from the IRAS Faint Source Survey flux-density limited at 200 mJy at 12 μm . A 12 μm local luminosity function is derived and, for the first time in the literature, effects of density variation in the local universe are considered and corrected in the calculation of the 12 μm luminosity function. It is also found that the 12 μm -selected sample are dominated by quasars and active galaxies, which therefore strongly affect the 12 μm luminosity function at high luminosities. The ultraluminous infrared galaxies are relatively rare at 12 μm comparing with a 25 μm sample.

Subject headings: infrared: sources – luminosity function

1. Introduction

The mid-infrared (MIR) spectral region is well-suited for studying starburst and ultraluminous galaxies. About 40% of the luminosity from starburst galaxies is radiated from 8-40 μm (Soifer et al. 1987). Extinction effects are small, and infrared cirrus emission is reduced at these wavelengths relative to far-infrared bands. For a fixed telescope aperture, the spatial resolution is also higher at shorter wavelengths, and the confusion limit lies at higher redshifts. All the recent and near-future infrared space missions, such as the *Infrared Space Observatory (ISO)*, the *Wide-Field Infrared Explorer (WIRE)*, and the *Space Infrared Telescope Facility (SIRTF)* will conduct surveys in mid-infrared bands. *WIRE*, a Small Explorer mission due to launch in late 1998 (Hacking et al. 1996; Schember et al. 1996), will conduct a very deep survey at 12 and 24 μm to study the evolution of starburst galaxies. To interpret the results of these surveys now in progress or soon to commence, it is necessary to better understand the mid-infrared properties of galaxies in the local Universe.

One of the most important tools for extracting the rate and type of galaxy evolution from a mid-infrared survey is the faint source counts. A local mid-infrared luminosity function is the basis for calculating the mid-infrared faint source counts incorporating different evolutionary scenarios, and to extract the evolution by comparing with observations. Mid-infrared luminosity functions have been calculated at 12 and 25 μm (Soifer & Neugebauer 1991) using a 60 μm selected IRAS sample (Soifer et al. 1987). More recently, Rush et al. (1993) selected a 12 μm flux-limited sample and calculated the luminosity functions for Seyfert and non-Seyfert galaxies in the sample. In a previous paper (Shupe et al. (1997), Paper I hereafter), we have presented the results of a 25 μm luminosity function calculated from a large flux-limited IRAS sample containing 1456 galaxies. We continue to select a flux-limited sample and calculate the luminosity function at 12 μm in this paper.

The relation between the mid-infrared color and luminosity plays another important role in estimating various properties of galaxy evolution. It defines distinct regions in the color-flux diagram, for example, for different types of evolution and for different populations of galaxies. Such a relation is indicated by the 12-25 μm vs. 60-100 μm color-color relation or by the 12-25 μm color vs. the far-infrared luminosity relation obtained from the IRAS survey (Soifer & Neugebauer 1991), and can be estimated from a large sample of galaxies selected at mid-infrared bands.

Emission features near 12 μm thought to be produced by aromatic hydrocarbon molecules have been observed in many astronomical spectra (e.g., Gillett et al. 1973; Russell et al. 1978; Sellgren 1984; Roche, Aitken, & Smith 1991; Boulade et al. 1996; Vigroux et al. 1996; Metcalfe et al. 1996; Cesarsky et al. 1996; Lu et al. 1997).

These broad emission features complicate the calculations of k -corrections and the fluxes and luminosities at mid-infrared bands. Fortunately, ISO observations have resulted in high-quality mid-infrared spectra in various astronomical circumstances, and the on-going surveys of IRAS galaxies using ISO can provide an especially useful handle on this problem.

In the next section we present a model to systematically calculate the contribution of the emission features in the mid-infrared bands of IRAS galaxies. The model is then incorporated in the following sections. Section 3 discusses the mid-infrared color-luminosity relation obtained from the large 25 μm -selected sample of Paper I. The population-dependency of the relation is discussed. Then we present the calculation of the 12 μm luminosity function in Section 4. We first discuss a selection of galaxy sample flux-limited at 12 μm from the IRAS Faint Source Survey in Section 4.1. Then the luminosity function is derived and corrected for density variations in Section 4.2. In Section 4.3 we discuss the effects of active galaxies and quasars on the 12 μm luminosity function. We summarize our results in Section 5.

2. Calculating the flux of the mid-infrared emission features and the k -correction

The mid-infrared spectral energy distributions of galaxies contain broad emission features, centered at 3.3 μm , 6.2 μm , 7.7 μm , 8.6 μm , and 11.3 μm , from very small grains. They have been interpreted as emission from aromatic hydrocarbons molecules (Léger & Puget 1984). Since the first detection of the narrow emission band at 11.3 μm by Gillet et al. (1973), the emission features have been found in many astronomical spectra, including those of infrared-quiet (e.g. Boulade et al. 1996) and starburst (e.g. Vigroux et al. 1996) galaxies. For more distant sources, the emission features are redshifted into and out of the IRAS bands, especially the 12 μm band. They significantly change the observed fluxes at these bands, and affect the k -correction and the calculations of the rest-frame fluxes and luminosities.

At this stage, we want to establish a simple model which can estimate the contribution of the emission to the IRAS in-band fluxes in a general way. Using the ISO PHT-S spectrometer, Lu et al. (1997) obtained the mid-infrared spectra of 16 nearby galaxies covering a range of far-infrared luminosities. Based on the data and a spectra template kindly provided by George Helou and Nanyao Lu at IPAC, we model the relation between the emission and the far-infrared color as a step function:

$$\frac{\text{EF}}{\text{FIR}} = \begin{cases} 0.12 & \text{if } F_\nu(60\mu\text{m}) < 0.6F_\nu(100\mu\text{m}) \\ 0.06 & \text{otherwise} \end{cases}, \quad (1)$$

where EF and FIR refer to the flux due to the four emission features at $6.2 \mu\text{m}$, $7.7 \mu\text{m}$, $8.6 \mu\text{m}$, and $11.3 \mu\text{m}$ (the $3.3 \mu\text{m}$ feature is not clearly detected for most of the 16 galaxies), and the far-infrared flux (defined as $1.26 \times 10^{-14}(2.58f_{60\mu\text{m}} + f_{100\mu\text{m}})$ watt m^{-2}), respectively, and F_ν is the flux density. The IRAS in-band relative flux of the emission features for a given galaxy at a given redshift is calculated using the spectra template and is then scaled according to the above relation to obtain the physical emission flux. The template spectrum we use will be published by Xu et al. (1998).

Our model is based on such a relation with far-infrared flux and color because, as shown by the results of Lu et al. (1997), the relative strength of the emission features (with respect to the far-infrared flux) appears to decrease with increasing starburst strength, characterized by the 60-100 μm color in the model. Physically, strong starburst activities can destroy small grains, thereby reduce their emission. These grains would also not survive if, say, there is strong enough activity in a galaxy nucleus. Our empirical model does not intend to discriminate between these phenomena.

The results by Lu et al. (1997) also show that the strength of the emission features relative to the mid-infrared (3 to $11.6 \mu\text{m}$) flux remains roughly constant ($\sim 50\%$) from galaxy to galaxy. This suggests that the continuum component within this wavelength range correlates with the emission features, and that they both have the same origin. It is possible that a blend of weak features by similar grains form most of the continuum (Moutou, Léger & d’Hendecourt 1996). The dominance of interstellar single-photon heating, which is typical when radiation intensity does not exceed some critical value (Boulanger et al. 1996), may have caused the general similarity of the emission spectra of normal galaxies. When radiation is strong enough, multiple-photon heating of small dust particles can contribute more significantly to the $12 \mu\text{m}$ continuum, as suggested by several ISO spectra of strong starburst regions (e.g. Vigroux et al. 1996 for the Antennae galaxies; Lutz et al. 1997 for M82). The grains can be destroyed by the radiation, and the remaining emission features can be swamped in the increased continuum in these regions.

The ratios of the fluxes of the four emission features to the IRAS $12 \mu\text{m}$ fluxes of the 16 galaxies are about 0.4 to 0.6. Therefore we would expect less than 60% relative corrections due to the emission features within the $12 \mu\text{m}$ IRAS band for nearby galaxies. This is our practical upper-limit for the relative flux due to the emission features. Figure 1 illustrates the distribution of the relative emission flux in the $12 \mu\text{m}$ band for the $25 \mu\text{m}$ selected sample containing 1456 galaxies discussed in Paper I. We identified (see Section 3) active galaxies from the others (“inactive galaxies” in the Figure) in the sample and show the corrections separately for these populations. It is seen that the peak correction due to the emission features is somewhat smaller for active galaxies, indicating stronger radiation

intensity around the grains in these galaxies. The overall average in-band flux from emission features is about 10 - 20% of the 12 μm flux. There are only 8 sources ($\sim 0.5\%$ of the sample) lying at the 60% limit, indicating that the model produces modest estimates for the emission flux for most of the sources.

For k -corrections at the IRAS 12 and 25 μm bands, we assume a power-law between the 12 and 25 μm continuum fluxes. The in-band emission flux (of the redshifted emission features) is first subtracted from the total in-band flux to estimate the power-law slope. After k -correction, the rest-frame in-band emission flux is added back to the continuum to give the corrected total flux. A more accurate treatment of correcting for the emission features will be discussed in our forthcoming paper (Xu et al. 1997), where we will present the SEDs and our evolutionary models based on the new k -correction.

3. The mid-infrared color-luminosity relation

There is a significant correlation between the mid-infrared 12-25 μm color and the far-infrared luminosity, as also suggested by the 12-25 μm vs. 60-100 μm color-color relation (Helou 1986; Soifer et al. 1987; Bothun, Lonsdale, & Rice 1989; Soifer & Neugebauer 1991). To explore a similar color vs. mid-infrared luminosity relation, we use the large 25 μm selected samples discussed in Paper I. We also incorporate the model discussed previously to calculate the fluxes and luminosities more accurately. The luminosities are calculated similarly as we did in Paper I.

A 25 μm selected all-sky sample may suffer from incompleteness due to large noises in 25 μm near the ecliptic plane. We have demonstrated in Paper I that our 1456-galaxy sample is highly complete across the ecliptic plane. We have also defined, in Paper I, a high-quality sample which has a higher 400 mJy flux density limit near the ecliptic region (the rest of the region is limited at 250 mJy). Here we want to compare the results of the color-luminosity relation for these different samples, and then we continue the analyses using the high-quality sample, which contains 1049 galaxies.

Since the samples are selected with moderate or high quality detections at 25 μm , some galaxies have upper limits for flux densities at 12 μm . Therefore the mid-infrared colors of these galaxies are so-called censored data (Feigelson & Nelson 1985; Schmitt 1985; Isobe et al. 1986). We use the standard Kaplan-Meier (K-M) estimator (Kaplan & Meier 1958) to calculate the average color at each (binned) luminosity, assuming that the censored data has a random distribution at that luminosity. The Buckley-James (B-J) linear regression (Buckley & James 1979) is also used to provide a linear interpretation of the color-luminosity

relation. It is calculated from the original data, not from the K-M estimates. We have used the survival analysis tools in the IRAF STSDAS/ANALYSIS/STATISTICS package to carry out the analysis.

We first study the relation between the 12-25 μm color and the 25 μm luminosity. Figure 2 compares the results for the high-quality sample and the entire 25 μm sample limited at 250 mJy. Here the monochromatic luminosities are expressed as νL_ν and have units of solar luminosities. The squares are the K-M estimates in each half-decade luminosity bin. There is clearly a correlation between the 12-25 μm color and the 25 μm luminosity. The results for the two samples are similar. The B-J linear regression gives indistinguishable slopes and intercepts for the linear interpretation. The B-J results for these and the subsequent analyses are listed in Table 1. This confirms a conclusion from Paper I that the 250 mJy-limited sample, while at lower signal-to-noise ratio than the high-quality sample, does not contain systematic flux or color errors.

Figure 3 shows the scattered color-luminosity data and the B-J linear regression for the high-quality sample. To examine whether there are any artificial factors in the relation caused by the proportionality of the 25 μm fluxes and luminosities, we also obtained the relation of the same color vs. 60 μm luminosity for the sample. The results are shown in Table 1. It turns out that the B-J slope hardly changes, while the intercept decreases, indicating a roughly constant 25 to 60 μm ratio as a function of luminosity, which was discovered earlier (Soifer & Neugebauer 1991). This confirms the reliability of the color vs. 25 μm luminosity relation. Furthermore, we have calculated the mid-infrared fluxes of the galaxies in the high-quality sample, according to the following definition, given by Xu & Buat (1995):

$$F_{mir} = F_{12\mu m} \frac{c\delta\lambda_{12\mu m}}{\lambda_{12\mu m}^2} + F_{25\mu m} \frac{c\delta\lambda_{25\mu m}}{\lambda_{25\mu m}^2}, \quad (2)$$

where F_{mir} , $F_{12\mu m}$, $F_{25\mu m}$ are mid-infrared flux, 12 μm and 25 μm flux densities, respectively, λ s are wavelengths, c is the speed of light, $\delta\lambda_{12\mu m} = 7\mu m$, and $\delta\lambda_{25\mu m} = 25\mu m$ are the band passes. $\delta\lambda_{25\mu m}$ is increased from the real IRAS band pass to cover the spectral range up to 40 μm . The resulting MIR color-luminosity relation is shown in Figure 4. The similar proportionality between the 12-25 μm color and the MIR luminosity and the scattering patterns exist, comparing with those in Figure 3. But this relation is more robust to error in the flux measurement in one of the MIR bands. The B-J regression results are listed in Table 1.

To study the distribution of different galaxian populations in the color-luminosity relation, we have obtained the morphology and type information for the sources in the high-quality sample from the NASA/IPAC Extragalactic Database (NED). In Figure 5 we

re-draw the same color-luminosity relation as in Figure 3, with the populations of QSOs, Seyfert 1 and 2s, and LINERs highlighted. The Seyfert 2s and LINERs appear to follow the B-J regression, but Seyfert 1s tend to fall below the regression line on average. There is a population of luminous quasars grouped below the regression line (very blue), indicating that they have relatively flat spectra. This causes the drop of the color values of the two highest luminosity bins in Figure 2. On the other hand, the nearby low luminosity infrared sources are redder, causing the deviation of the color-luminosity relation in the first few bins in Figure 2.

To further investigate the effects of different populations on the color-luminosity relation, we exclude the Seyfert galaxies, LINERs, and quasars from the sample and calculate the K-M average and B-J regression for the rest of the galaxies, which are essentially starburst galaxies and luminous infrared galaxies (defined as $L_{fir} \gtrsim 10^{11}L_{\odot}$). Figure 6 compares the results with those obtained for all populations. The linear regression for the infrared luminous quasars is also shown by the dotted line. The average slope of the color-luminosity relation becomes greater for the starburst population. At high-luminosity bins, the average colors of the starburst galaxies become systematically redder, and much redder than those of the quasars. We notice that there is a color turn-over at the $10^{12}L_{\odot}$ bin, but statistical significance is poor with only two sources in that bin. Higher luminosity bins are completely occupied by quasars in our sample. This relation implies that very high luminosity starburst systems, if they exist, could be distinguished from quasars by their 12-25 μm color.

We have also obtained the blue magnitudes for 1390 galaxies in our entire 250 mJy-limited sample. These magnitudes were obtained from the following catalogs in order of preference: the CfA redshift catalog, the COSCAT, and the NED. We then calculated the relation between the 12-25 μm color and the ratio of the far-infrared and the blue luminosity, which indicates the starburst strength. Figure 7 shows the B-J linear regression with all populations included. The active galaxies and quasars are indicated similarly as in Figure 5. The figure shows that a good correlation exists between these colors. Different populations, including Seyfert 1 galaxies and the infrared luminous quasars, appear to follow the same linear regression. A single 12-25 μm color vs. L_{fir}/L_b relation appears to apply equally to the different populations. To examine this, we have re-calculated the K-M average and B-J regression for the population of starburst galaxies only (excluding Seyfert galaxies, quasars, and LINERs). The results are shown in Figure 8. The 12-25 μm color- L_{fir}/L_b relations for the starbursts and all populations are essentially the same. As mentioned in Section 2, starbursts and activities in the galactic nuclei can have a similar effect on the grain emission. The L_{fir}/L_b is a good strength indicator (see below) for the starburst population, whereas the color vs. 25 μm luminosity is more sensitive to these

different populations. We also obtained the 12-25 μm color vs. L_{mir}/L_b relation using the definition of the mid-infrared flux in Equation 2, and the results are similar to Figure 7.

The 12-25 μm color vs. 25 μm luminosity relation in Figure 6 provides powerful tools in recognizing different populations such as starbursts, luminous and ultraluminous infrared galaxies, and quasars. Infrared luminous quasars can be easily identified by their bluer colors in the diagram. The luminous and ultraluminous infrared galaxies would generally have redder colors at high-luminosity bins in such a relation. Although different populations are well-mixed in the color-color relation of Figure 8, the ultraluminous infrared galaxies also segregate themselves in such a relation, as suggested by the proportional relation between the ratio L_{fir}/L_b and L_{fir} , found by Soifer et al. (1987). Figure 9 demonstrates such a segregation. In the Figure, we have identified the luminous and ultraluminous infrared galaxies (excluding active galaxies and quasars) with $L_{\text{fir}} \geq 10^{11}L_{\odot}$ (filled squares) among the rest of the population. It is seen that all galaxies in this population have greater L_{fir}/L_b ratios. They can be selected from high L_{fir}/L_b bins with high probability. For example, among 224 sources with $\log_{10}(L_{\text{fir}}/L_b) > 1$ in the Figure, 133 sources have $L_{\text{fir}} \geq 10^{11}L_{\odot}$, and 100 of them are luminous and ultraluminous infrared galaxies. The ease of detecting such luminous star-forming galaxies is what makes modest-sized infrared telescopes such effective probes of galaxy evolution in the early universe, compared to the strong selection effects that complicate optical and UV studies.

The Seyfert galaxies, on the other hand, are more difficult to identify, although the difference in the linear regressions in Figure 6 is partly due to this population (Seyfert 1s are mostly below the regression lines). The luminous Seyfert galaxies are also more scattered in the 12-25 μm color vs. L_{fir}/L_b ratio relation than the ultraluminous infrared galaxies, increasing the probability of identifying the latter at high L_{fir}/L_b ratio bins.

4. The local luminosity function at 12 μm

4.1. Sample Selection

We based our sample on a selection from the IRAS Faint Source Survey (FSS; Moshir et al. 1992). The main data product of the FSS is the Faint Source Catalog (FSC) and the Faint Source Reject File. The Faint Source Reject File contains possible detections that were not included in the FSC for assorted quality-control reasons.

Subsamples can be drawn from the FSS-based sample flux-limited at 250 mJy at 25 μm discussed in Paper I. A 12 μm flux-limited subsample drawn directly from that sample, however, would suffer from two biases. First, since we used moderate or good quality

detection criterion in the 25 μm sample, galaxies with moderate or good quality detections at 12 μm may not have the same or better detection qualities at 25 μm , and therefore would not be included in such a subsample. The second source of incompleteness for such a subsample comes from a color bias: sources which satisfy the 12 μm flux-density criterion may not have 25 μm flux densities greater than 250 mJy, thereby would be excluded. On the other hand, we want to stay close to the spatial and color selection criteria which defined the highly complete 25 μm sample (see Paper I for discussions of the completeness of the sample). We therefore used the following criteria:

$$\begin{aligned}
 &F_\nu(12) \geq 200\text{mJy}; \\
 &\text{moderate or good quality detection at } 12\mu\text{m}; \\
 &|b| \geq 30^\circ, \text{ and not in Strauss et al. (1990) excluded zone;} \\
 &F_\nu(25) < F_\nu(60) \text{ and } F_\nu(12) < 2F_\nu(25), \text{ or} \\
 &F_\nu(60) < F_\nu(25) < 1.6F_\nu(60) \text{ and } F_\nu(12) < F_\nu(25).
 \end{aligned}$$

The 90% completeness limit for the FSC lies at a 12 μm flux density of 180 mJy for sky covered by 2 HCONs, and at 150 mJy for coverage of 3 HCONs, for $|b| > 10^\circ$ (Moshir et al. 1992). Here the flux-density limit of 200 mJy is chosen because it gives the sample a high redshift-completeness (see below).

1059 sources in the FSC meet the above criteria. We found 619 galaxies which are in the 25 μm sample from Paper I with redshifts. We matched the rest of the sources with the 1.2 Jy Survey catalog, the November 1993 public version of J.P. Huchra’s ZCAT, the NED database, and the SIMBAD database. This process resulted in an addition of 43 galaxies with redshifts, 3 galaxies with no redshift information, and the identification of the rest of the sources as non-galaxies (mostly stars).

We have applied our selection criteria to the Faint Source Reject File and found 101 sources. We followed the same matching techniques as we used in Paper I to find galaxies from the Reject File and found 6 galaxies, all with redshifts. A sample of 101 sources randomly distributed in the same sampling region would result in less than one match with galaxies. This gives a total of 668 galaxies with redshifts in our final sample, and the redshift completeness of the sample is 99.5%.

The 1.2 Jy Survey catalog also provides the ADDSCAN flux densities for the sources extended at 60 μm . For those sources which have no ADDSCAN flux densities in the 1.2 Jy Survey but are extended at 12 μm , we obtained their ADDSCAN flux densities by running XSCANPI. These ADDSCAN flux densities are used in the calculation of the 12 μm luminosity function.

In Figure 10 we illustrate a number vs. flux test to examine the completeness of our sample. It is seen that the source counts in different flux-density bins fall close to the line with the slope -1.5, expected for a homogeneous flux-limited sample of galaxies. There is no indication of incompleteness of the sample down to 200 mJy.

The model discussed in Section 2 is incorporated to estimate the k -corrections. The relative flux due to the emission features between 3 μm and 11.6 μm is peaked at $\sim 18\%$, similar to the features in Figure 1.

4.2. Luminosity function results

To calculate the luminosity function for the sample, we have used secondary distances when available. Otherwise, a linear Virgocentric inflow model (Aaronson et al. 1982) and a Hubble constant of $75 \text{ km s}^{-1} \text{ Mpc}^{-1}$ is used. (Based on the same reasons we outlined for the 25 μm selected sample in the Appendix of Paper I, we note that our estimated luminosities here can be simply scaled if a different Hubble constant is used.) We have followed the same criteria as Soifer et al. (1987) to identify Virgo cluster galaxies (with a distance of 17.6 Mpc).

We have calculated the 12 μm luminosity function of the sample using the $1/V_{max}$ estimator, the non-parametric maximum-likelihood method, and the parametric maximum-likelihood method with the Yahil et al. (1991) robust parametric form. As discussed in Paper I, the $1/V_{max}$ estimator is potentially affected by the inhomogeneities of the large-scale spatial distribution of the sources in the sample. The maximum-likelihood methods assume that the spatial and luminosity distributions are independent, so that the shape of the luminosity function can be determined without being affected by any spatial structures, whereas the normalization of the function is lost. In this paper, we normalize these luminosity functions to the total number of sources in our sample.

Figure 11 shows the results. The luminosity function is plotted in the form of a visibility function (luminosity function multiplied by a factor of $L^{2.5}$), which has the advantage of showing the relative numbers of galaxies in a flux-limited sample. The results of the $1/V_{max}$ estimator agree with those of the non-parametric maximum-likelihood method within the $1\text{-}\sigma$ errors, although at high luminosity bins the non-parametric maximum-likelihood method gives higher values at the first few bins then drops off, and the error bars become very large in these bins. The large uncertainty in these bins is one disadvantage of the method when dealing with small numbers of sources. The results of the parametric maximum-likelihood method, however, show a steep slope after the peak and do not agree at higher luminosity

bins. (The parameters are: $C = 0.00252$, $\alpha = 0.2648$, $\beta = 2.6372$, $L_\star = 4.9215 \times 10^9 L_\odot$, using the same definitions as in Yahil et al. 1991 and Paper I) This indicates that this parametric form may not apply to the 12 μm luminosity function.

The standard V/V_{max} test (Schmidt 1968) examines whether the spatial distribution of the sources in a sample is uniform. The circles in Figure 12 shows the result for the sample. The $1/V_{max}$ estimator is affected by the variations of the V/V_{max} values shown in the plot. Following the techniques discussed in Paper I, we have calculated a radial density distribution for the galaxies in the sample using the non-parametric maximum-likelihood method. We have corrected the $1/V_{max}$ estimator and the V/V_{max} test using the radial density distribution. There is marginal improvement on the values of V/V_{max} (heavy dots) which are now closer to 0.5, shown in Figure 12. The corrected $1/V_{max}$ luminosity function, normalized to the total number of sources in the sample, is shown in Figure 13, where the same maximum-likelihood results are also plotted. The visibility function becomes smoother at low luminosity bins, while the flattening at the high luminosity bins is somewhat more significant.

We have also derived the 12 μm luminosity function from the 25 μm local luminosity function (Paper I) using a bi-variate luminosity function technique. Define $\rho_{12}(L_i)$ and $\rho_{25}(L_j)$ as the 12 μm and 25 μm luminosity functions at luminosity bins L_i and L_j (assuming the same binning size), respectively, and $P_{i,j}$ as the conditional probability of finding galaxies with the luminosity L_i at 12 μm and the luminosity L_j at 25 μm . Then

$$\rho_{12}(L_i) = \sum_j P_{i,j} \rho_{25}(L_j). \quad (3)$$

The probability $P_{i,j}$ is calculated empirically (non-parametric) from the 25 μm flux-limited sample, taking into account also the information content of 12 μm upper limits using the Kaplan-Meier estimator (Schmitt 1985; Feigelson and Nelson 1985). Using the parametric maximum-likelihood estimate of the 25 μm luminosity function, which agrees well with the non-parametric maximum-likelihood and the density-corrected $1/V_{max}$ results as discussed in Paper I, we obtained the 12 μm luminosity function, shown by the squares in Figure 13. While the results match the $1/V_{max}$ estimates reasonably well at high luminosity bins, they are lower at low luminosity bins, agreeing with the maximum-likelihood estimates. The greater estimates of the density-corrected $1/V_{max}$ method in these bins are probably due to the left-over effect caused by structures in the local density distribution, seen in the density-corrected V/V_{max} test results (heavy dots in Figure 12). Caution should be taken when using the $1/V_{max}$ estimates of the 12 μm luminosity function at these luminosity bins. We have obtained the $1/V_{max}$ luminosity function and the V/V_{max} test results calculated for the southern sky subsample (265 galaxies at $b < -30^\circ$). The V/V_{max} test shows that

the subsample is fairly homogeneous, namely the mean V/V_{max} are consistent with 0.5 for different flux limits and different $L_{12\mu m}$ bins (see also Paper 1). Therefore the luminosity function should not be affected by the local structure significantly. There is good agreement between the bi-variate luminosity function and the $1/V_{max}$ luminosity function of the southern subsample, both are below the density-corrected $1/V_{max}$ luminosity function at low luminosities.

It should be pointed out that given the small size of the southern subsample, the luminosity function calculated from it has relatively large statistical uncertainties. On the other hand, the bi-variate luminosity function also has larger error bars due to the additional uncertainties introduced in the calculation of the probability $P_{i,j}$, in particular at both ends of the $25 \mu m$ luminosity where the number of galaxies in each bin is very small. Potentially, it may also miss any population which is present in $12 \mu m$ but absent in $25 \mu m$, although we do not see any evidence for this.

We have compared the redshift distribution expected by the estimated luminosity function with the one given by the sample. The observed redshift distribution can be corrected by the maximum-likelihood estimate of the radial density distribution to remove the effect of density inhomogeneities (see Paper I). In Figure 14, the dashed and solid line histograms show the distributions before and after the density correction, respectively. We can see that structures such as Virgo cluster represented by the peak at ~ 17 Mpc are suppressed and the redshift distribution becomes smoother after the density correction. The dotted line is the prediction by the density-corrected $1/V_{max}$ luminosity function, which fits the solid histogram rather well.

The results of the $1/V_{max}$ luminosity functions before and after the density correction are listed in Table 2. We do not include a reliable parametric estimate for the $12 \mu m$ luminosity function, since the flattening at high luminosity bins is difficult to account for by the current parametric forms.

4.3. Luminous galaxies at $12 \mu m$

The flattening of the $12 \mu m$ visibility function at high luminosity bins is unlikely due to the mid-infrared emission features. We have calculated the visibility function of the $12 \mu m$ continuum from a subsample drawn from the current sample with the flux density of the continuum (i.e. the flux density with the mid-infrared emission features removed) limited at 200 mJy. The result indicates that the flattening tail still remains without the emission features.

As discussed in Section 2, the strength of the continuum appears to correlate with that of the nearby emission features. If they have the same origin, both can be reduced in regions where radiation intensities are high, in which case multiple-photon heating of small dust particles can contribute more significantly to the 12 μm continuum. For luminous galaxies with strong radiation, significant effect on their 12 μm fluxes from the emission features is therefore quite unlikely.

The flattening effect is most probably due to the dominance of a population of Seyfert galaxies and quasars in these bins. Among the 15 galaxies with $L_{12\mu\text{m}} \geq 10^{11}L_{\odot}$, for example, there are 6 galaxies having the morphology of either a Seyfert 1 or a Seyfert 2 galaxy, 6 quasars, 1 BL LAC object, and 2 luminous infrared galaxies. The Seyfert galaxies and quasars dominate the high luminosity bins at 12 μm . The ultraluminous infrared galaxies are scarce at these luminosities. A 12 μm flux-limited sample selects favorably the active galaxies and quasars, especially at high luminosities. It is therefore essential to use longer wavelength bands, such as 25 μm , to detect ultraluminous infrared galaxies. Spinoglio & Malkan (1989) also showed that the 12 μm fluxes remain approximately a constant 25% of the bolometric flux for all types of Seyfert galaxies and quasars. A complete 12 μm -selected sample of these galaxies is therefore also complete to some bolometric flux.

We have identified the active galaxies (including Seyfert galaxies, BL LACs, and quasars) in our sample using NED. They form a flux-limited subsample of 109 galaxies. We obtained the 12 μm luminosity function for this subsample, shown by the circles in Figure 15. Previously, Rush et al. (1993) obtained the luminosity functions for Seyfert and non-Seyfert galaxies. Their samples were also 12 μm -selected but under different criteria. Figure 15 shows their 12 μm luminosity function of the Seyfert galaxies (dashed line) for comparison. In the same Figure, we also compare our $1/V_{max}$ luminosity function (without density variation correction) for the entire population with their result. The Seyfert galaxies in their sample also dominate the high luminosity bins, shown by the merging of the functions at these bins. There is good agreement between our results, except at low luminosities for the samples including all galaxies. Since the local supercluster can introduce overestimates of the luminosity function in these luminosity bins, our density-corrected results should be more reliable, as discussed in Section 4.2.

5. Summary and conclusions

Our main results are summarized as follows:

1. Quasars and Seyfert galaxies dominate the high luminosity regime in a 12 μm

flux-limited sample. The ultraluminous infrared galaxies are relatively rare at 12 μm (contrast to a 25 μm sample).

2. We have a technique for differentiating between quasars and ultraluminous infrared galaxies using their 12-25 μm color (see Figures 5-9). Qualitatively, quasars are bluer than the luminous and ultraluminous infrared galaxies at high 25 μm luminosities. The ultraluminous infrared galaxies also have greater far-infrared to blue luminosity ratio on average than those of the other populations.

3. A highly complete sample flux-density limited at 200 mJy at 12 μm selected from the Faint Source Survey catalogs is used to calculate a local 12 μm luminosity function, which is then corrected for density-variation.

We are establishing a library of galaxy SEDs as a function of luminosity for more accurate k -corrections, and will discuss the faint source counts based on our 12 and 25 μm luminosity functions in a forthcoming paper (Xu et al. 1997).

We are grateful to George Helou and Nanyao Lu at IPAC for providing us with the results of the mid-infrared emission features of 16 galaxies observed by ISO and the spectra template. We thank Carol Lonsdale and Tom Soifer for helpful discussions. We wish to thank an anonymous referee and our editor, Greg Bothun, for making helpful comments. The SIMBAD database is maintained by CDS in Strasbourg, France. The NED database is supported at IPAC by NASA.

REFERENCES

- Aaronson, M., Huchra, J., Mould, J., Schechter, P. L., and Tully, R. B. 1982, ApJ, 258, 64.
- Bothun, G. D., Lonsdale, C. J., & Rice, W. 1989, ApJ, 341, 129.
- Boulade, O. et al. 1996, A&A, 315, L85.
- Boulanger, F. et al. 1996, A&A, 315, L325.
- Buckley, J. and James, I. 1979, *Biometrika*, 66, 429.
- Cesarsky, D. et al. 1996, A&A, 315, L305.
- Feigelson, E. D. and Nelson, P. I. 1985, ApJ, 293, 192.
- Gillett, F. C., Forrest, W. J., and Merrill, K. M. 1973, ApJ, 183, 87.
- Hacking, P. B. et al. 1996, The Wide-Field Infrared Explorer (WIRE) Mission, to appear in International Symposium on Diffuse Infrared Radiation and the IRTS, Institute

- of Space and Astronomical Sciences, Sagamihara, Japan.
- Hacking, P. B., Condon, J. J., and Houck, J. R. 1987, *ApJ*, 316, L15.
- Hacking, P. B., and Soifer, B. T. 1991, *ApJ*, 367, L49.
- Helou, G. 1986, *ApJ*, 311, L33.
- Isobe, T., Feigelson, E. D., and Nelson, P. I. 1986, *ApJ*, 293, 192.
- Kaplan, E. L. and Meier, P. 1958, *J. Am. Stat. Assoc.* 53, 457.
- Léger, A. and Puget, J. L. 1984, *A&A*, 137, L5.
- Lu, et al. 1997, *BAAS*, 28, 1356.
- Lutz, D. et al. 1997, *preprint*.
- Metcalf, L. et al. 1996, *A&A*, 315, L105.
- Moshir M., et al. 1992, *IRAS Faint Source Catalog Explanatory Supplement, Version 2*.
- Moutou, C., Léger, A., and d’Hendecourt, L. 1996, *A&A*, 310, 297.
- Roche, P. F., Aitken, D. K., & Smith, C. H. 1991, *MNRAS*, 252, 282.
- Rush, B., Malkan, M. A., and Spinoglio, L. 1993, *ApJS*, 89, 1.
- Russell, R. W., Soifer, B. T., and Willner, S. P. 1978, *ApJ*, 220, 568.
- Schember, H., Kemp, J., Ames, H., Hacking, P., Herter, T., Fafaul, B. Everett, D., Sparr, L. 1996, “The Wide-Field Infrared Explorer (WIRE)”, *SPIE Proceedings*, 2744, *Infrared Technology and Applications XXII*, p. 751-760.
- Schmidt, M. 1968, *ApJ*, 151, 393.
- Schmitt, J. H. M. M. 1985, *ApJ*, 293, 178.
- Sellgren, K. 1984, *ApJ*, 277, 623.
- Shupe, D. L., Fang, F., Hacking, P. B., and Huchra, J. P. 1997, *ApJ*, submitted (Paper I).
- Soifer, B. T. et al. 1987, *ApJ*, 320, 238.
- Soifer, B. T., & Neugebauer, G., 1991, *AJ*, 101, 354.
- Strauss, M., Davis, M., Yahil, A., & Huchra, J. P. 1990, *ApJ*, 361, 49.
- Vigroux, L. et al. 1996, *A&A*, 315, L93.
- Xu, C. and Baut, V. 1995, *A&A*, 293, L65.
- Xu, C. et al. 1997, *ApJ*, submitted.
- Yahil, A., Strauss, M. A., Davis, M., & Huchra, J. P. 1991, *ApJ*, 372, 380.

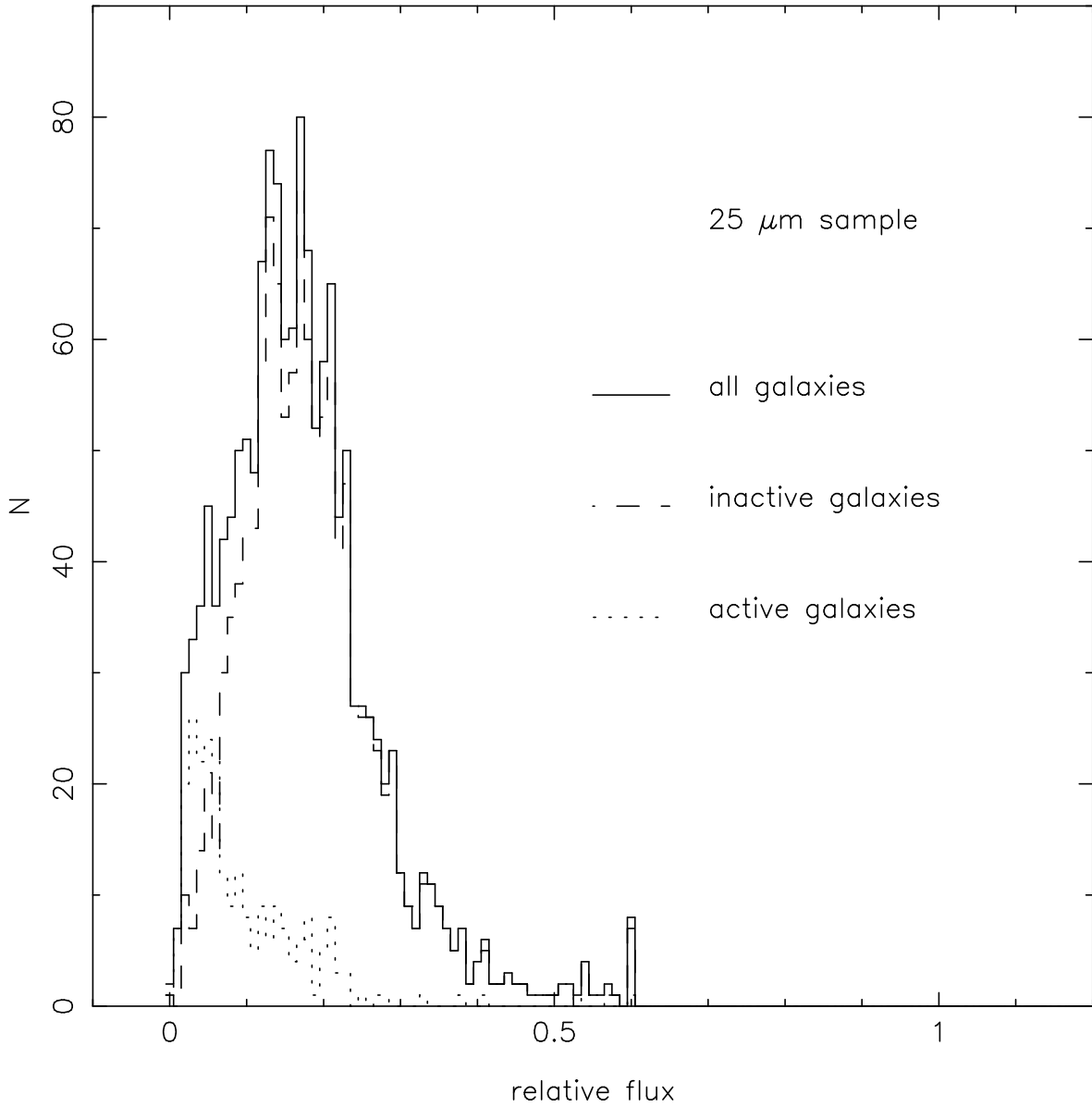


Fig. 1.— The histogram of the flux due to the (redshifted) emission features within the IRAS $12\ \mu\text{m}$ band relative to the $12\ \mu\text{m}$ flux, according to the model discussed in Section 2. The result is shown for a sample selected at $25\ \mu\text{m}$, discussed in Paper I (solid histogram), and its subsamples of active galaxies (dotted histogram) and the rest of the population – “inactive galaxies” (dashed histogram). The overall average relative flux is about 10-20%. The maximum relative flux is prescribed to be 60%.

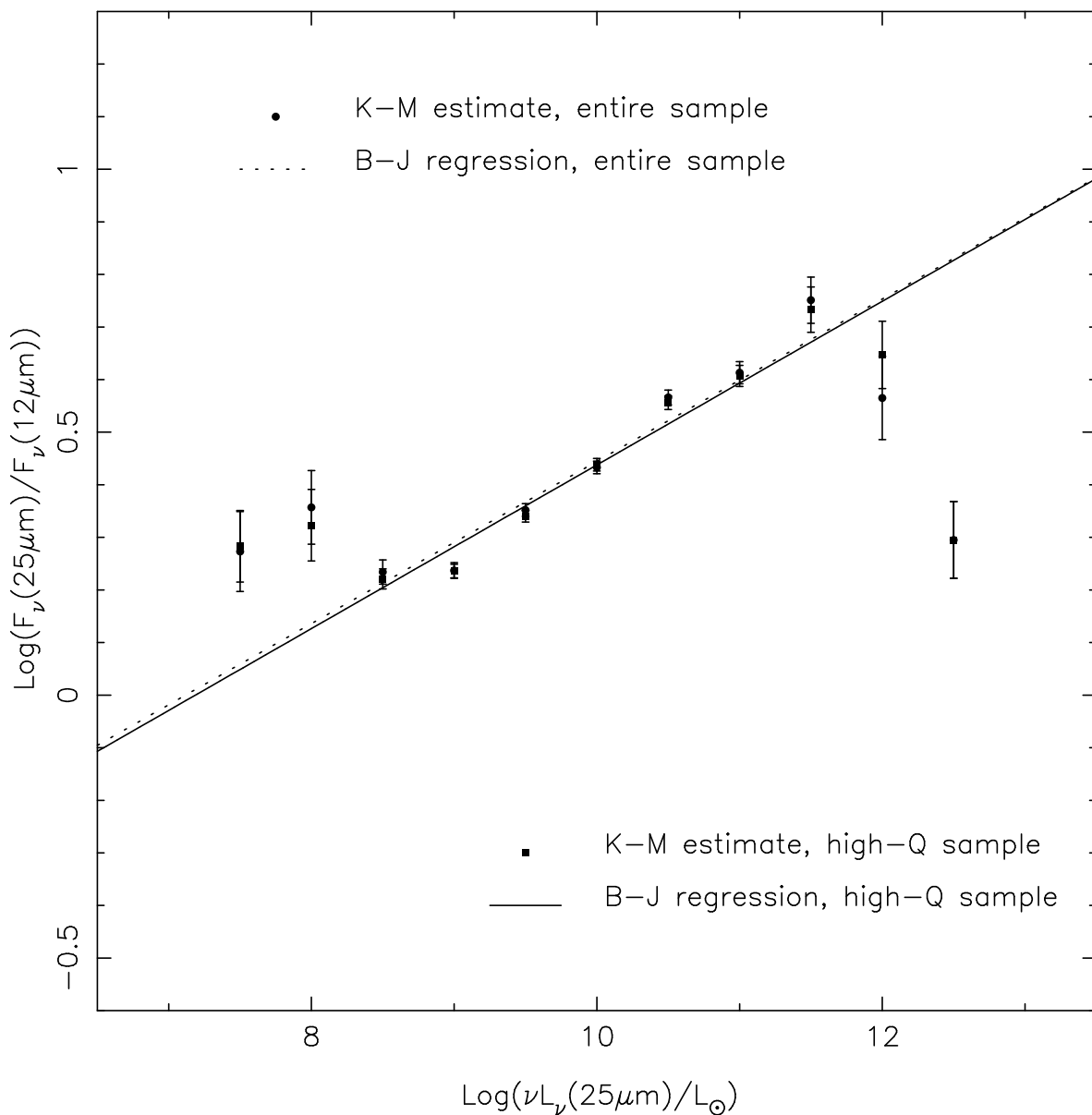


Fig. 2.— The 12–25 μm color vs. 25 μm luminosity relation for the entire 25 μm limited sample and the high-quality sample discussed in Paper I. The heavy dots show the Kaplan-Meier estimates of the mean colors in the half-decade luminosity bins for the entire sample, and squares for the high-quality sample. The solid and dotted lines are the Buckley-James linear regressions of the color-luminosity relation for the high-quality and the entire samples, respectively. The results are nearly identical for the two samples.

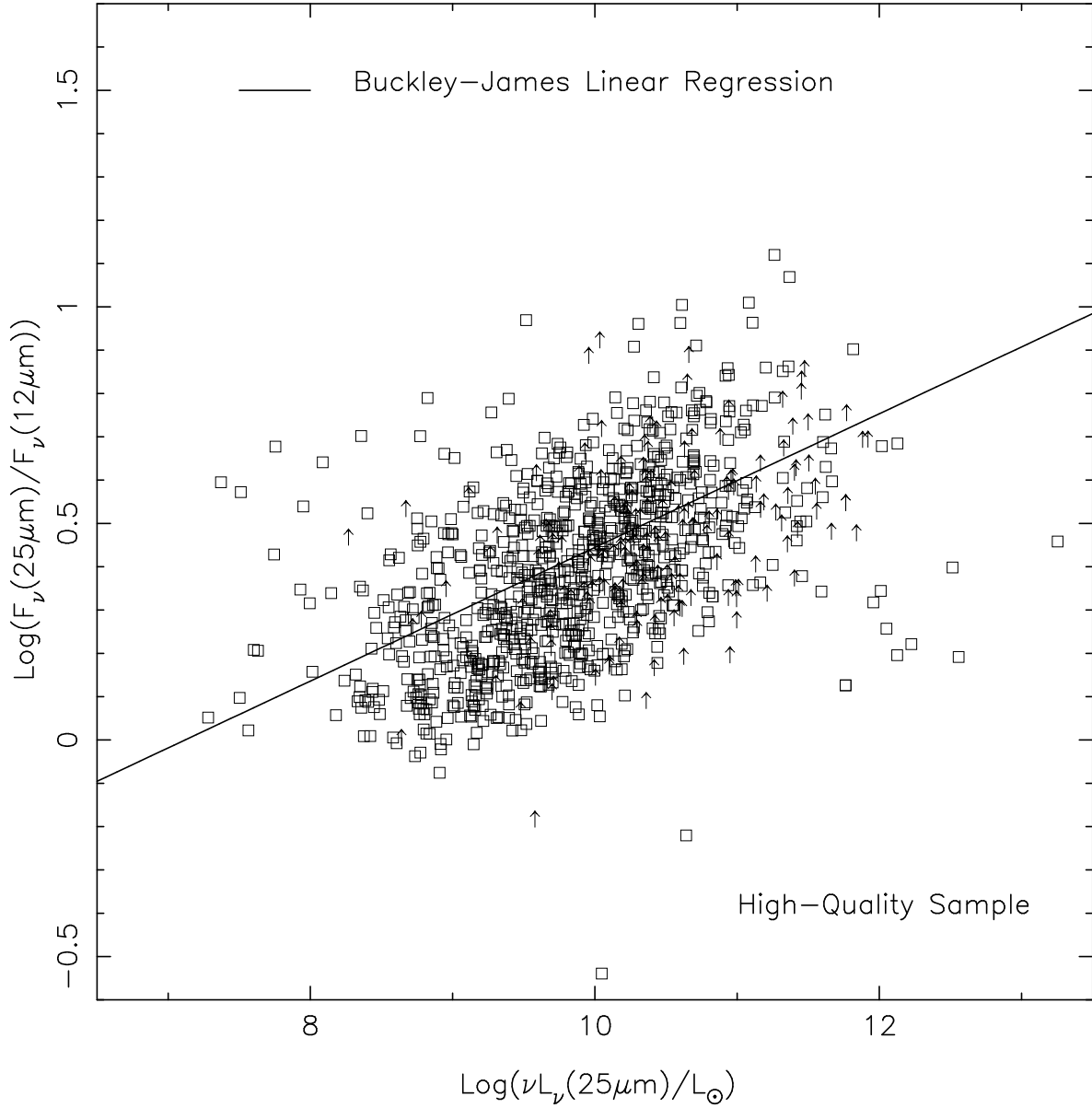


Fig. 3.— The scattered diagram for the 12-25 μm color vs. 25 μm luminosity relation obtained using the high-quality 25 μm selected sample. Arrows indicate the upper-limit detections at 12 μm . The solid line is the Buckley-James linear regression, the same as the dashed line in Figure 2.

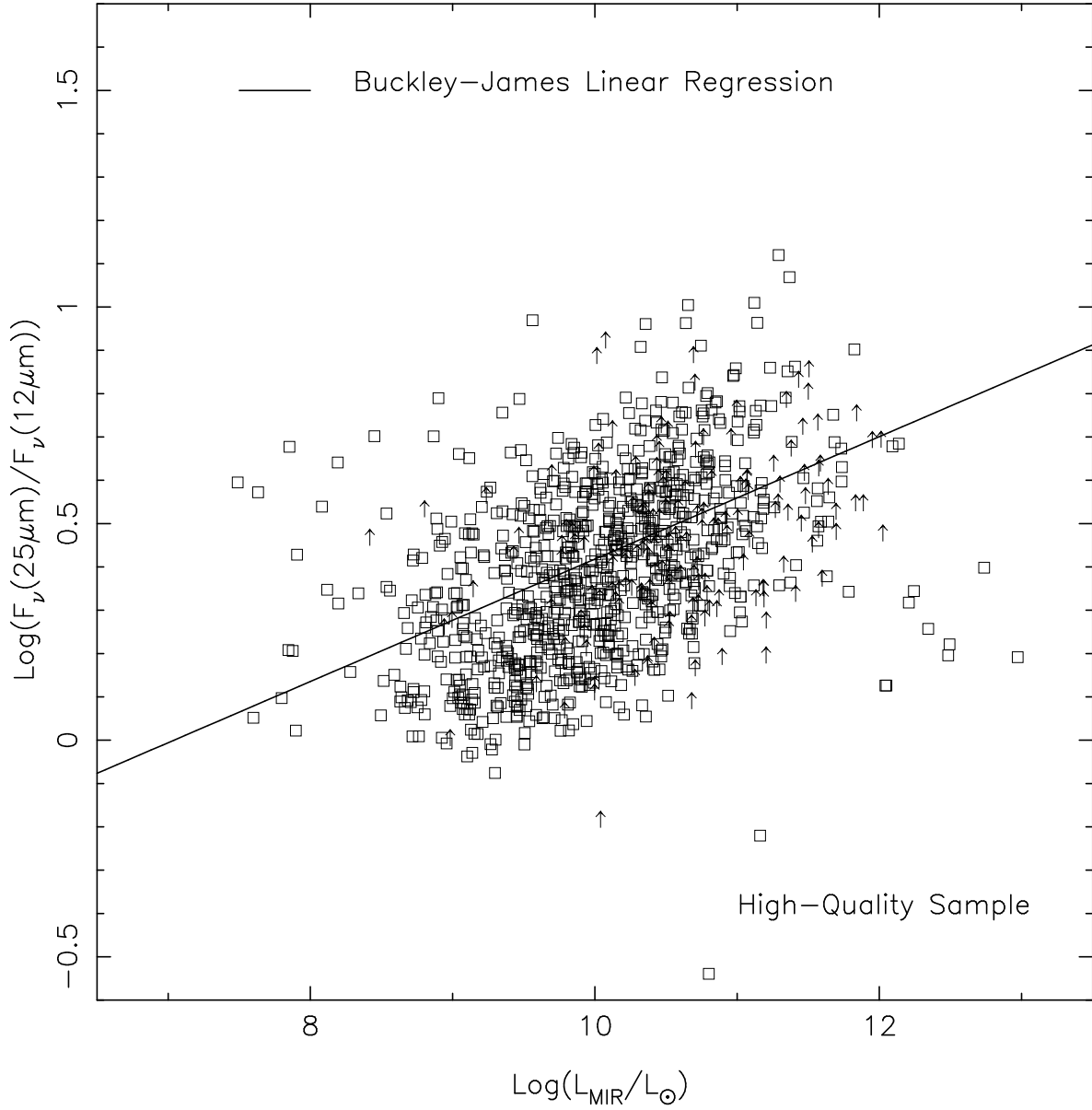


Fig. 4.— The 12-25 μm color vs. the mid-infrared luminosity relation obtained for the 25 μm high-quality sample. The mid-infrared flux is defined in the text. The scattering patterns are similar to those in Figure 3.

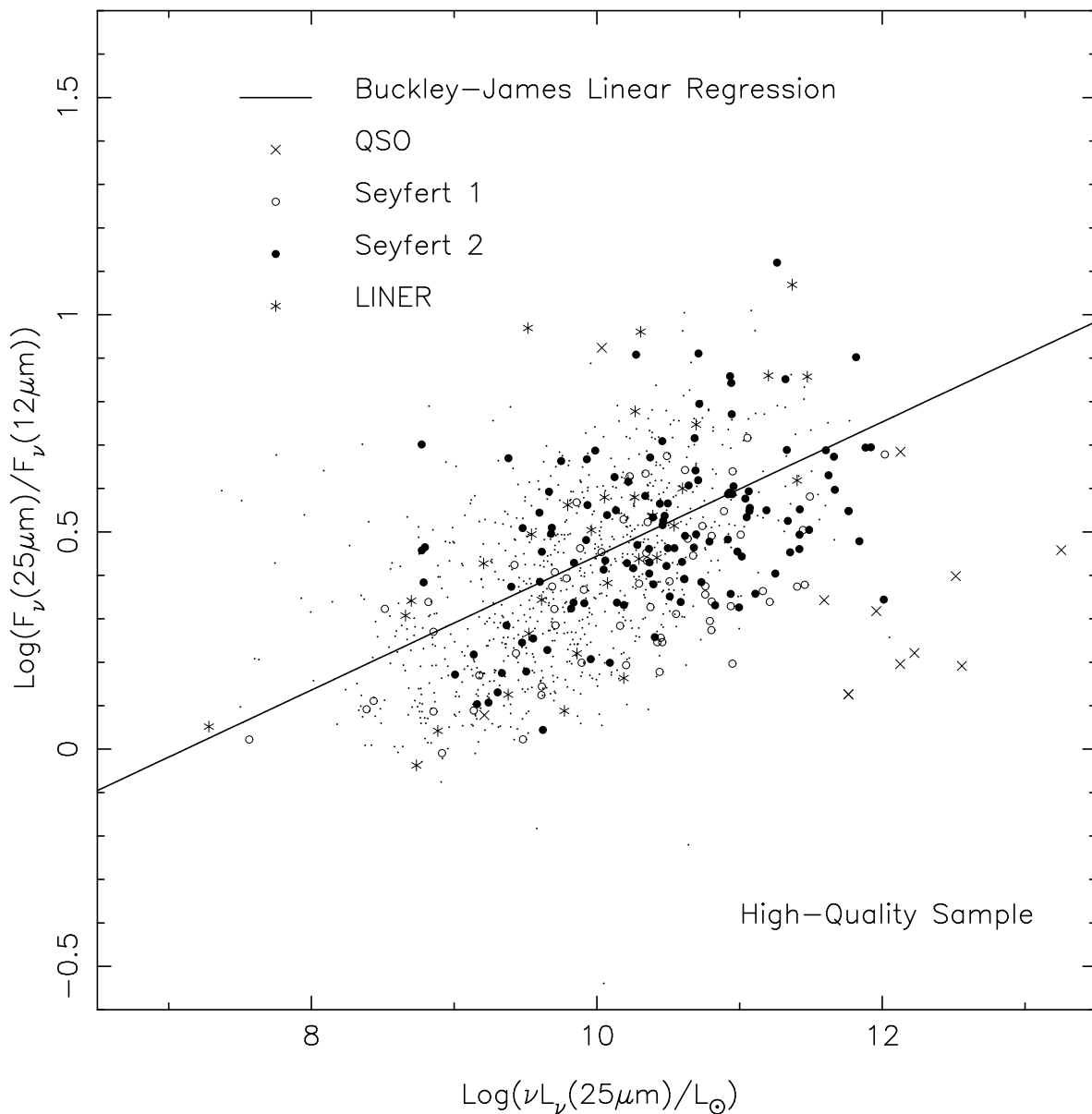


Fig. 5.— The populations of Seyfert galaxies (circles for Seyfert 1s, heavy dots for Seyfert 2s), QSOs (crosses), and LINERs (stars) in the same color-luminosity relation as in Figure 3. All the other galaxies are indicated by light dots. A population of infrared-luminous quasars has systematically bluer color and groups together below the Buckley-James linear regression line.

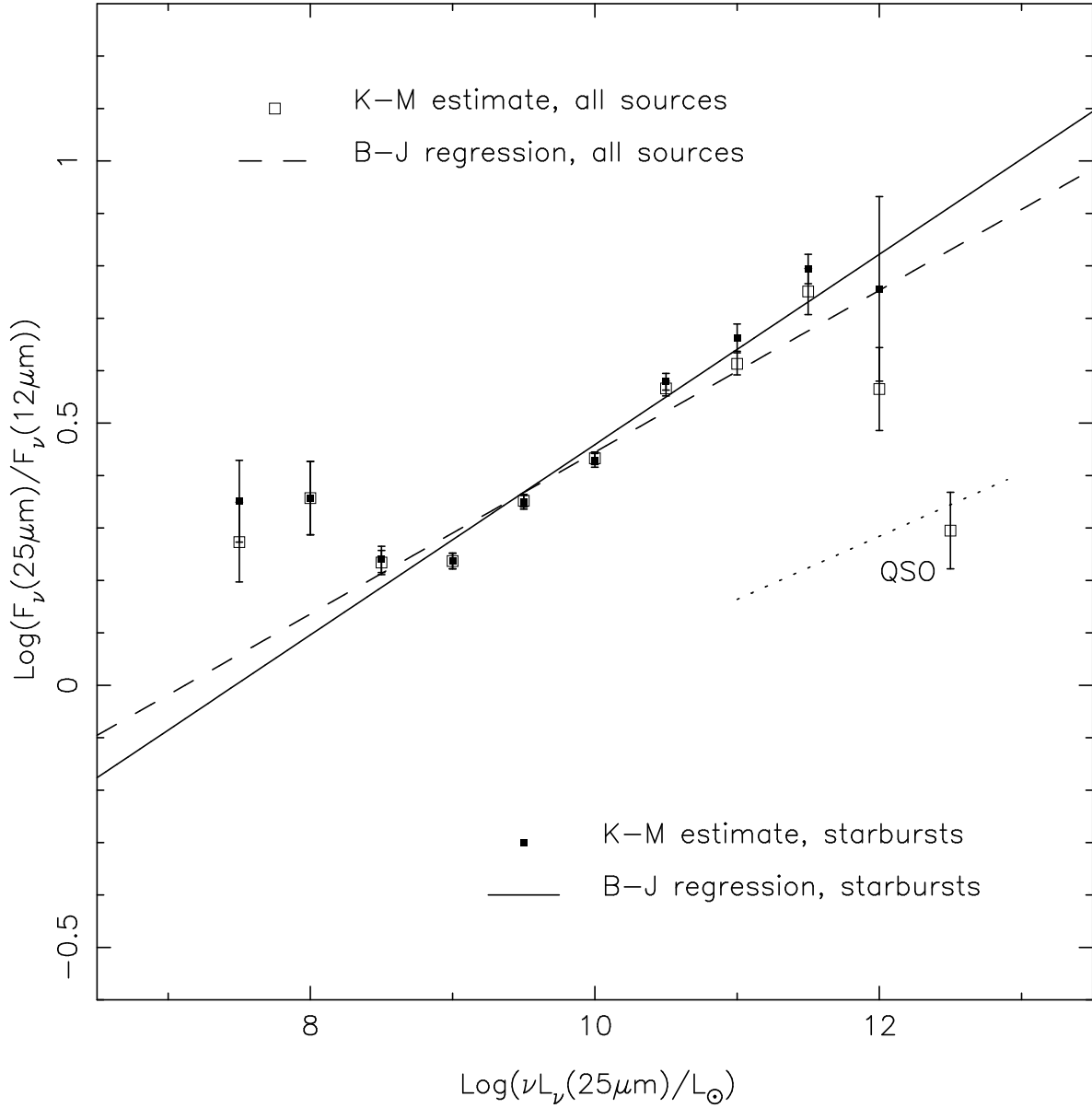


Fig. 6.— The Kaplan-Meier estimate and the Buckley-James linear regression of the color vs. $25\ \mu\text{m}$ luminosity relation. Empty squares and dashed lines show the result for the whole population and filled squares and solid lines for the starburst galaxy population. The dotted line is the linear regression for the luminous quasars.

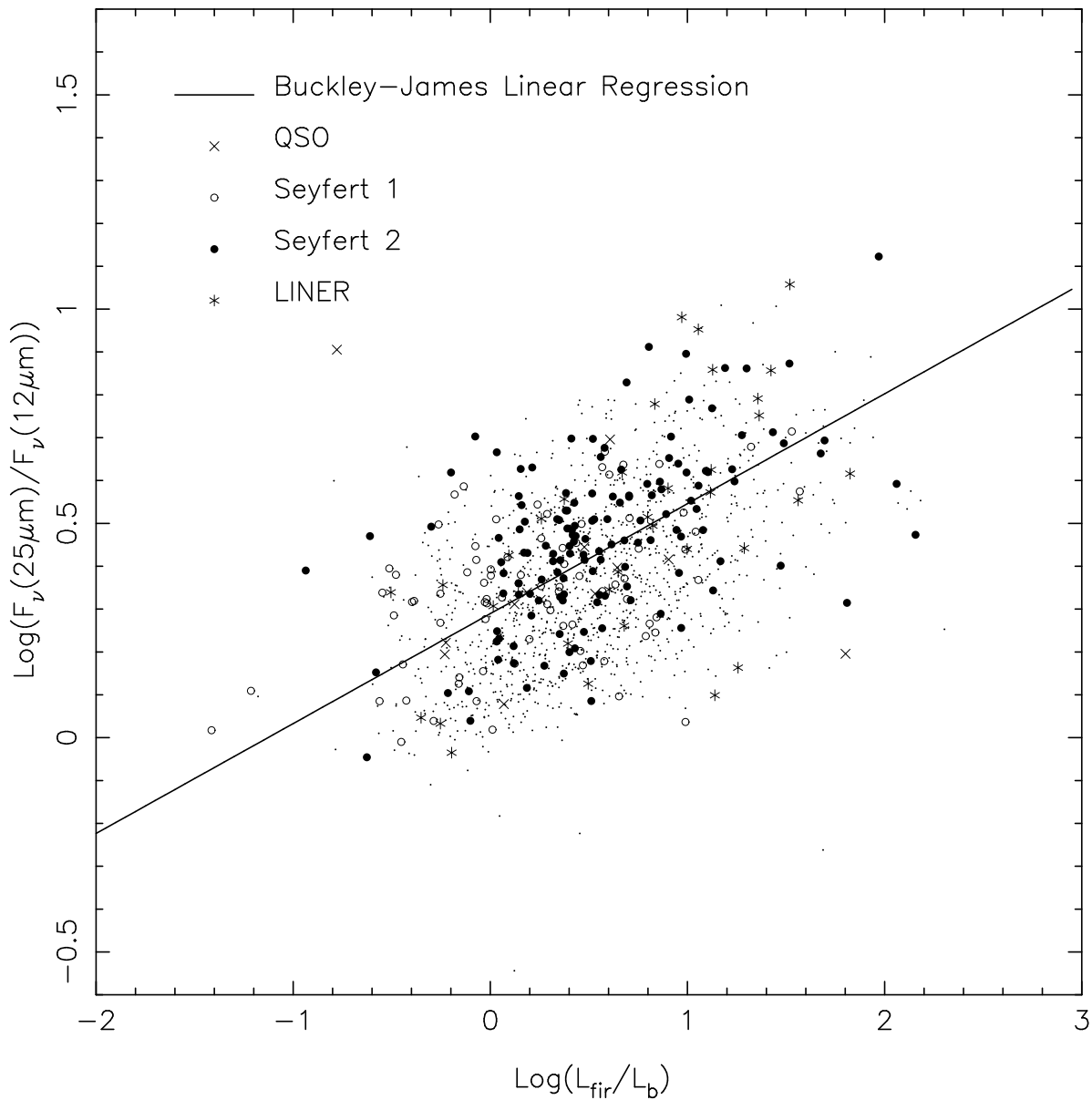


Fig. 7.— The scattered diagram for the relation between the 12-25 μm color vs. the ratio of far-infrared and the blue luminosities, with the same populations in Figure 5 indicated. The quasars identified in Figure 5 now distribute around the linear regression line, indicating their greater blue luminosities.

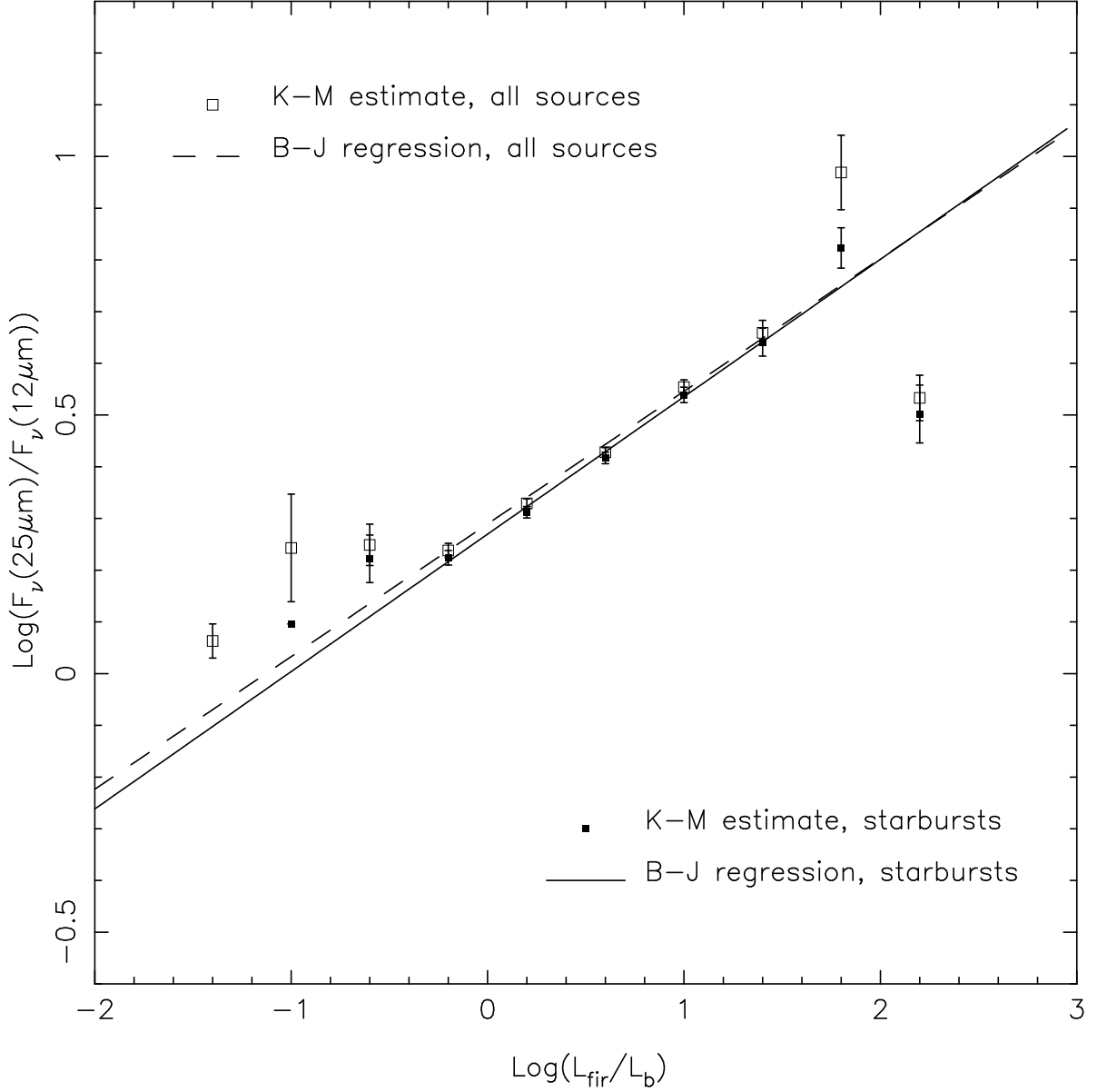


Fig. 8.— The Kaplan-Meier estimate of the average 12-25 μm color vs. the ratio of far-infrared and blue luminosities. The squares show the K-M average colors at the given L_{fir}/L_b bins. The empty squares are calculated for all sources, and the filled squares for starburst galaxies only. The dashed and solid line show the Buckley-James linear regression for all sources and for starbursts, respectively. The blue magnitudes are obtained for 1390 galaxies in the 25 μm -limited sample, as described in the text.

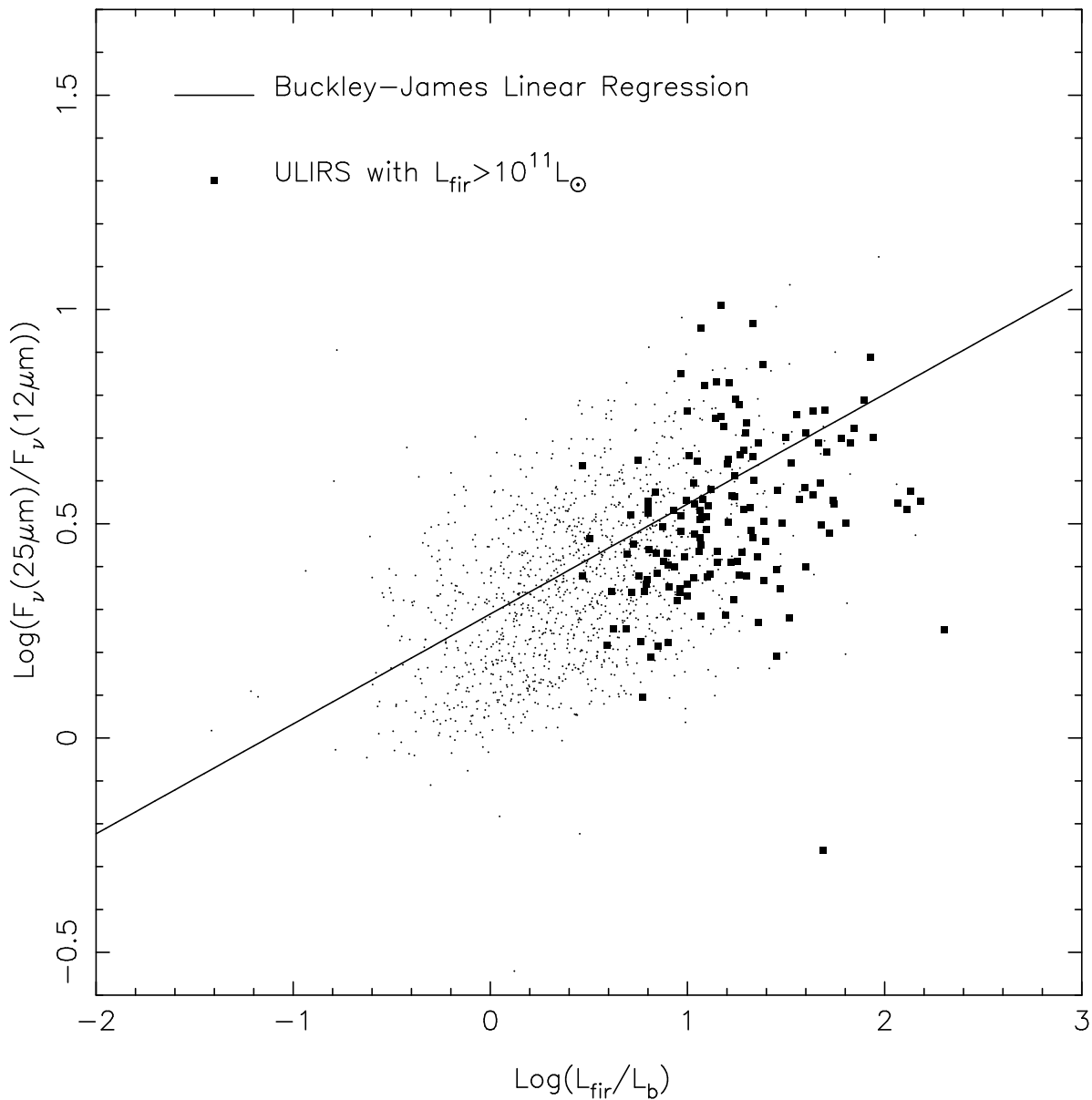


Fig. 9.— The same color-luminosity relation as in Figure 7 with the luminous and ultraluminous infrared galaxy population (ULIRS, $L_{\text{fir}} \geq 10^{11} L_{\odot}$) identified (filled squares). The rest of the sources are indicated by light dots. It is clearly seen that the luminous and ultraluminous infrared galaxies occupy the region with high $L_{\text{fir}}/L_{\text{b}}$ ratios.

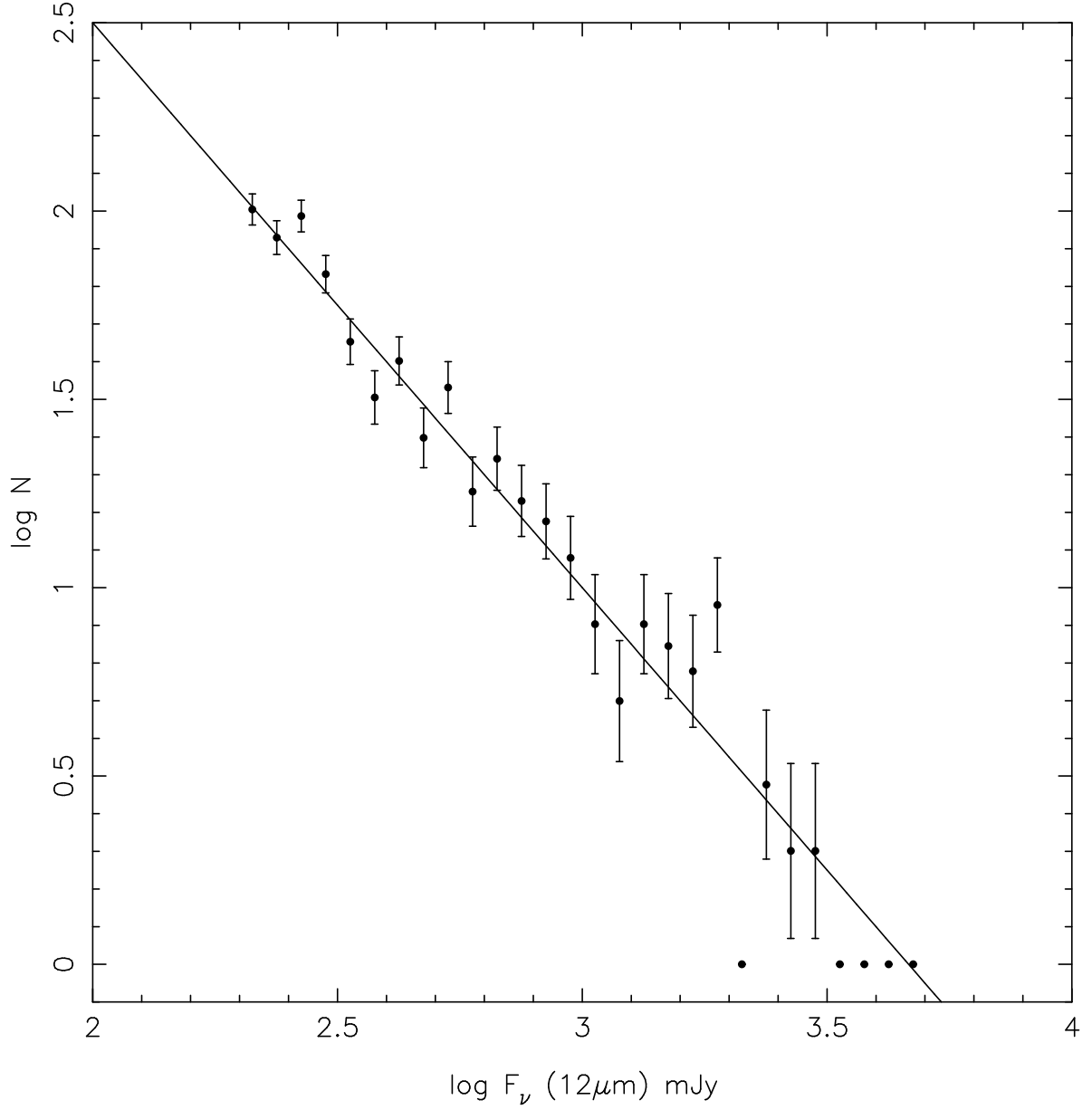


Fig. 10.— The number-flux test for the $12 \mu\text{m}$ selected sample flux-density limited at 200 mJy. For a complete, spatially homogeneously distributed sample, the relation should have a slope of -1.5, the solid line. The sample closely follows this relation.

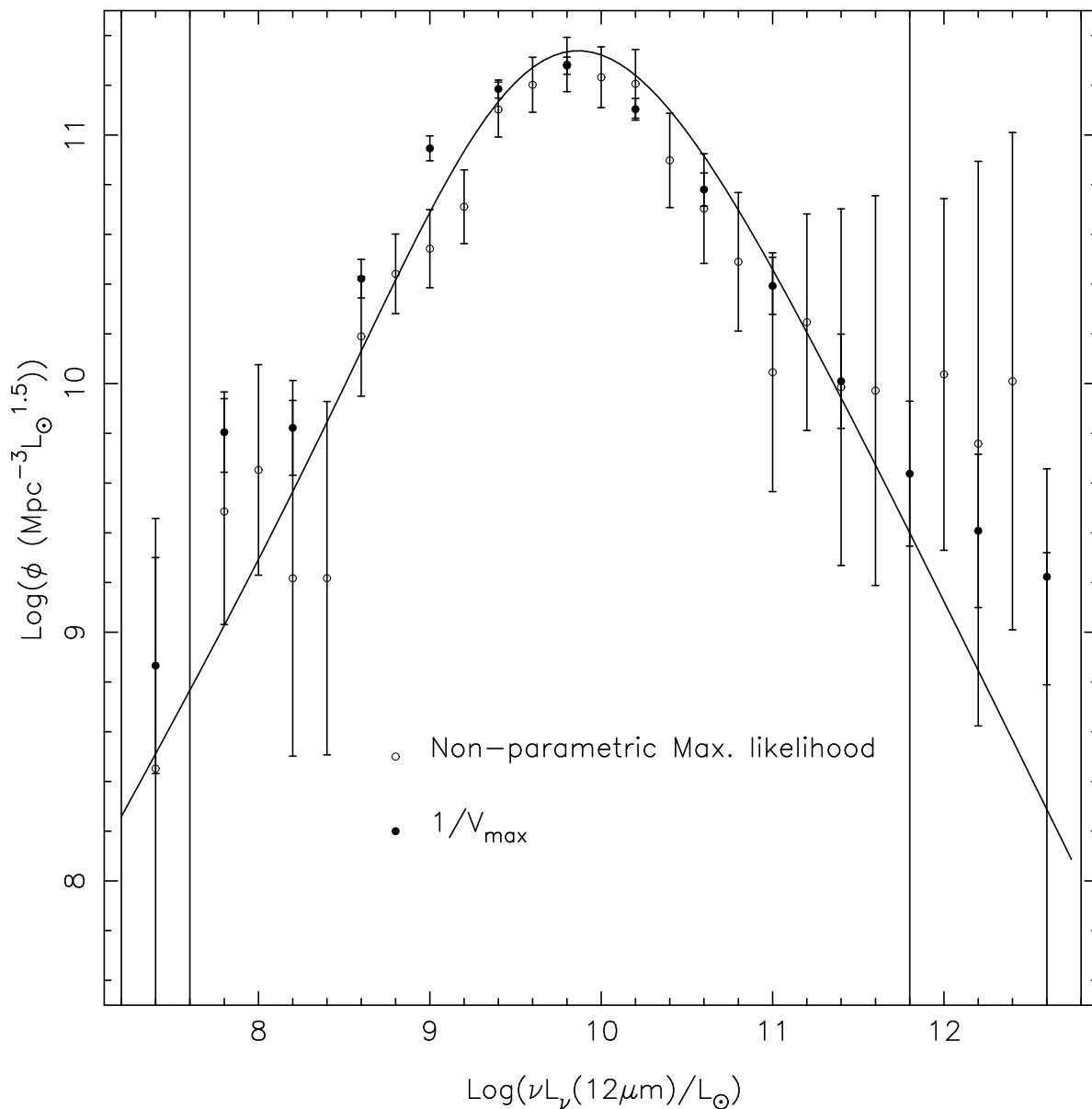


Fig. 11.— The 12 μm visibility function calculated using the $1/V_{\text{max}}$ estimator (heavy dots), the parametric (solid line) and the non-parametric (circles) maximum-likelihood methods. The parametric form of Yahil et al. (1991) is used. It does not fit the flattened high-L end of the other estimates. The maximum-likelihood estimates are normalized to the total number of sources in the sample. The 1- σ error bars are shown.

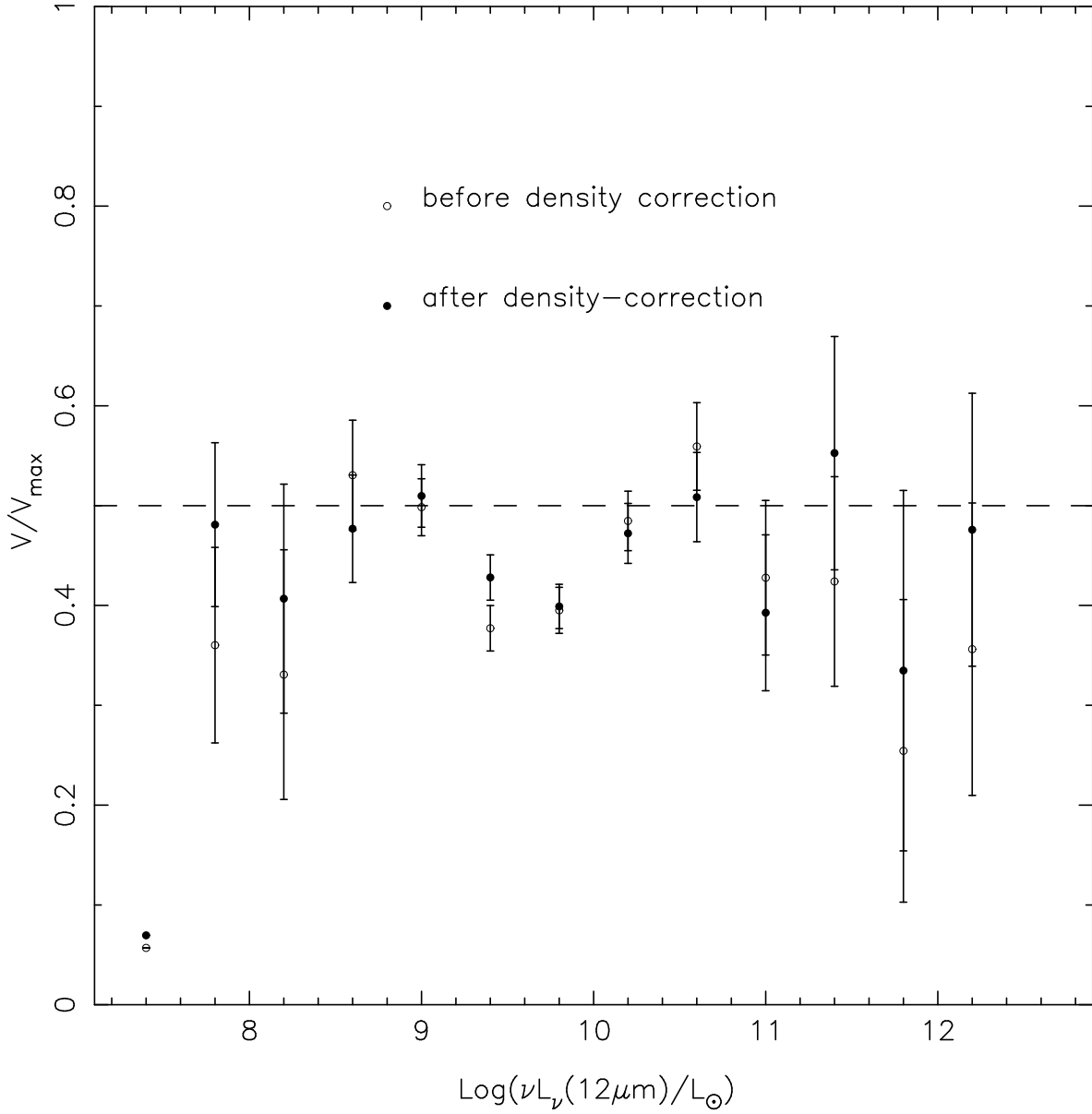


Fig. 12.— The V/V_{max} test for the 12 μm sample. Results are shown for both before (circles) and after (heavy dots) the corrections for the radial density inhomogeneities. The values of V/V_{max} are closer to 0.5 after the density correction, which indicates the better quality of the $1/V_{\text{max}}$ estimates in Figure 13.

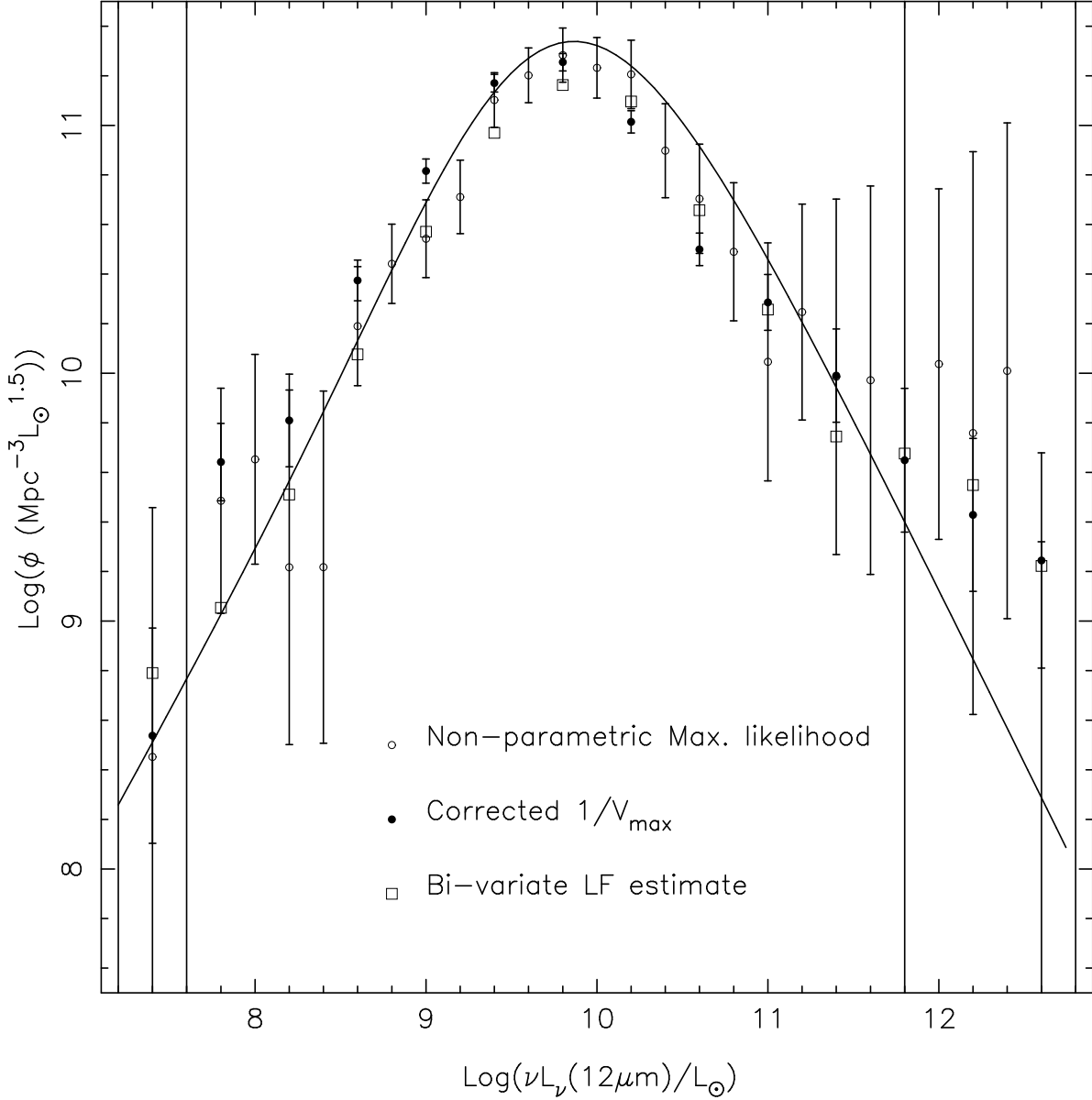


Fig. 13.— The $1/V_{max}$ 12 μm visibility function after the density correction (heavy dots). It is normalized to the total number of sources in the sample. Also shown are the maximum-likelihood estimates of Figure 11, and the 1-σ error bars. Squares show the results using a bi-variate function technique which derives the 12 μm luminosity function from the 25 μm one in Paper I.

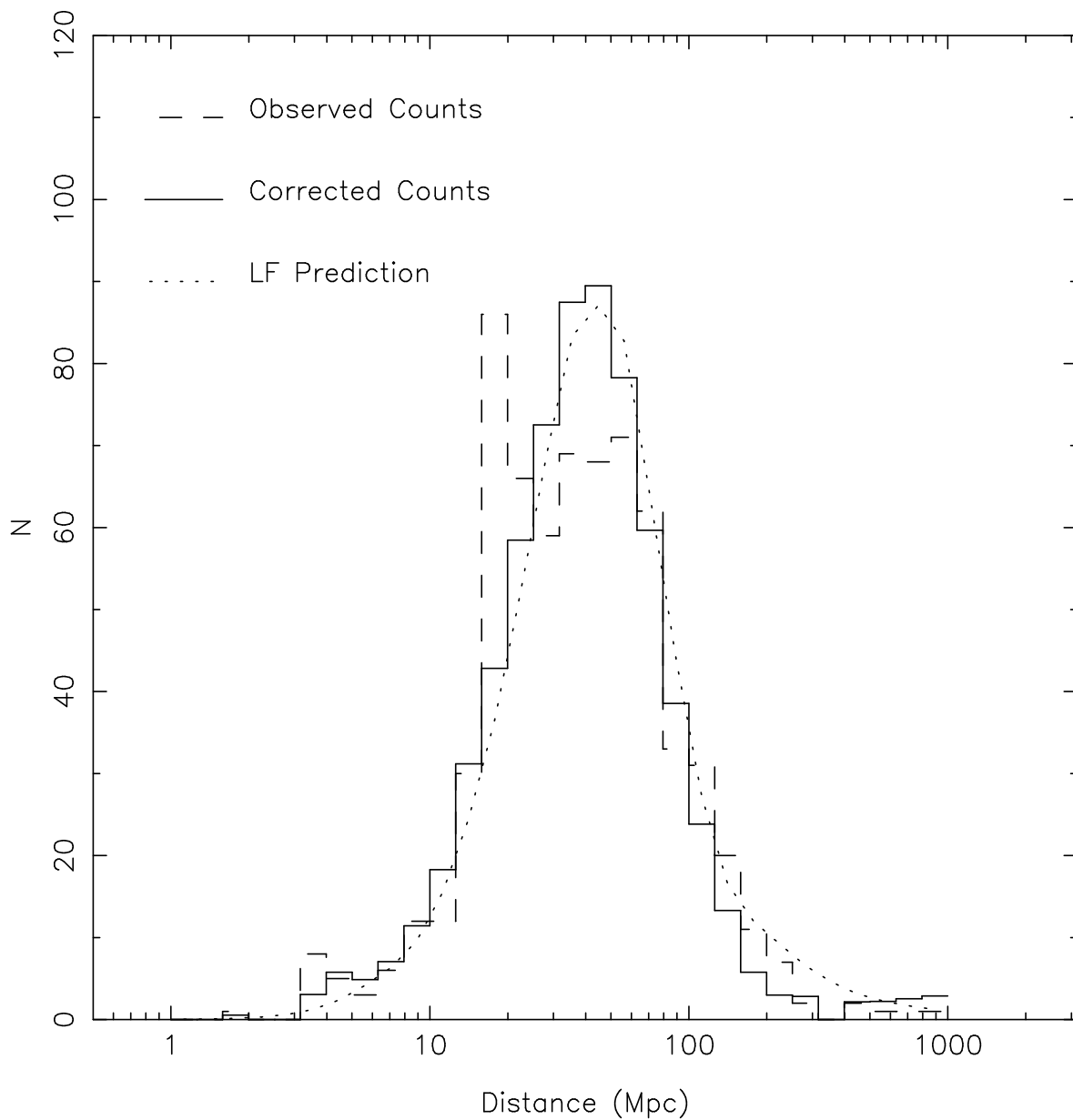


Fig. 14.— The redshift distribution of the sources in the $12\ \mu\text{m}$ sample. The observed distribution (dashed-line histogram) and the distribution after the radial density correction (solid-line histogram) are shown. The dotted line is a prediction by the density-corrected $1/V_{max}$ luminosity function in Figure 13.

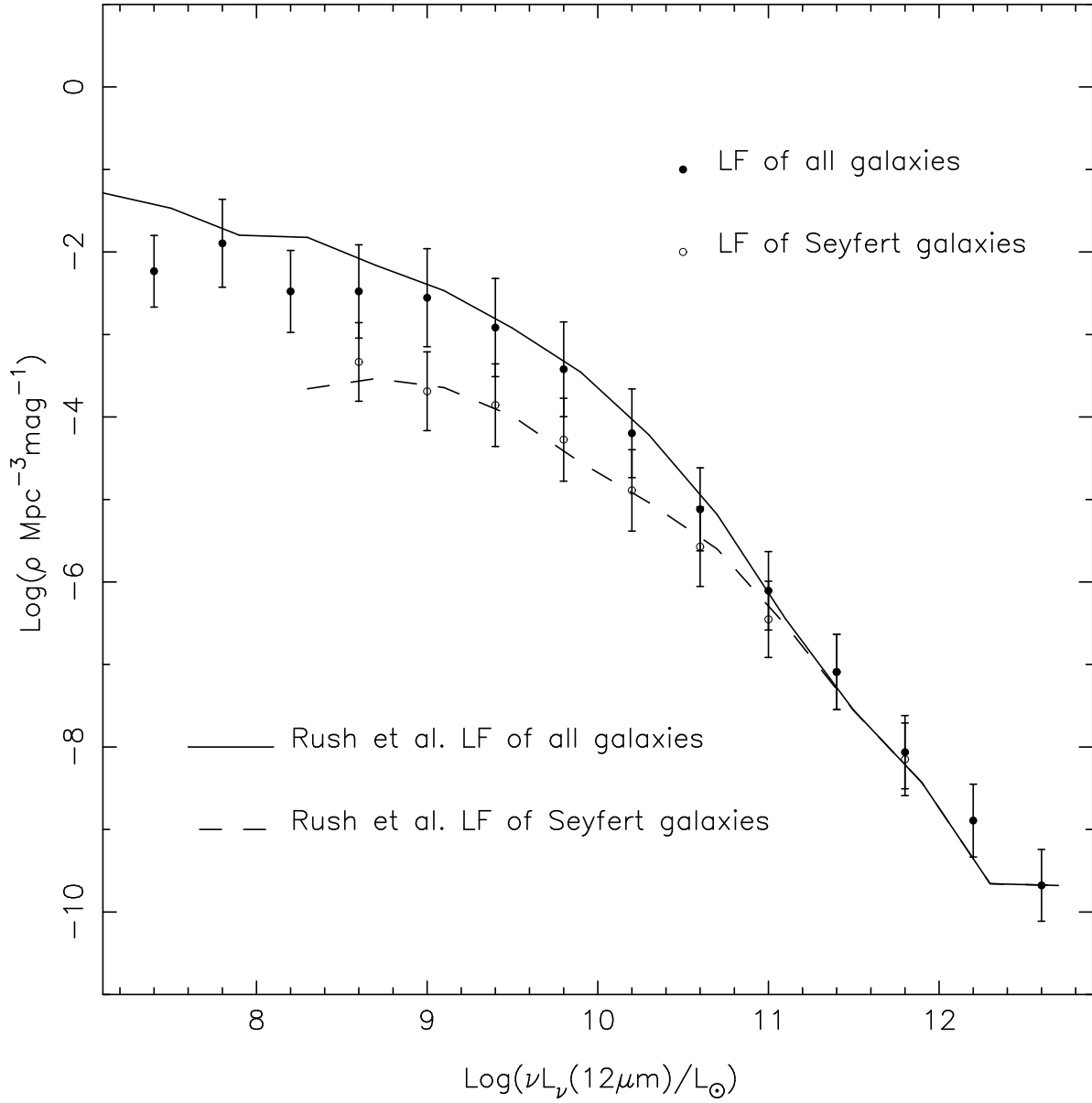


Fig. 15.— The 12 μm luminosity functions of all populations of galaxies (heavy dots) and Seyfert galaxies (circles) of our sample comparing with the ones (lines) obtained by Rush et al. (1993). Density variation correction is not performed for any of the data. The 1σ error bars are shown for our results.

Table 1. Results of the Buckley-James Linear Regression¹

X in $\log(F_{25\mu m}/F_{12\mu m}) = S \times \log(X) + I$	slope S	intercept I
$X = \nu L_{25\mu m}$, whole sample	0.1556	-1.1183
$X = \nu L_{25\mu m}$	0.1543	-1.0989
$X = \nu L_{60\mu m}$	0.1587	-1.2114
$X = L_{MIR}$	0.1413	-0.9949
$X = L_{fir}/L_b$	0.2565	+0.2894
$X = \nu L_{25\mu m}$, starbursts	0.1815	-1.3560
$X = \nu L_{25\mu m}$, luminous quasars	0.1203	-1.1595
$X = L_{fir}/L_b$, starbursts	0.2657	+0.2697

¹All relations are calculated using the 25 μ m-selected high-quality sample except for the first one, which uses the entire 25 μ m-selected sample, and the ones with L_{fir}/L_b ratio, for which the blue magnitudes are obtained for 1390 sources in the entire 25 μ m sample.

Table 2. $1/V_{max}$ Luminosity Functions

$\log(\nu L_\nu(12\mu\text{m})/L_\odot)$	before density correction		after density correction	
	$\log(\phi \text{ Mpc}^{-3})$	1σ error	$\log(\phi \text{ Mpc}^{-3})$	1σ error
7.4	-2.2340	-2.2340	-2.4621	-2.5621
7.8	-1.8952	-2.3251	-1.9585	-2.5032
8.2	-2.4780	-2.8358	-2.3908	-2.8570
8.6	-2.4781	-3.2257	-2.4256	-3.2489
9.0	-2.5541	-3.4929	-2.5844	-3.6320
9.4	-2.9154	-3.9942	-2.8297	-4.0138
9.8	-3.4214	-4.5240	-3.3453	-4.5385
10.2	-4.1968	-5.1940	-4.1859	-5.2694
10.6	-5.1198	-5.9324	-5.3002	-6.2212
11.0	-6.1068	-6.6860	-6.1141	-6.8001
11.4	-7.0907	-7.4510	-7.0098	-7.4734
11.8	-8.0624	-8.2356	-7.9510	-8.2264
12.2	-8.8921	-9.0408	-8.7717	-9.0204
12.6	-9.6769	-9.6769	-9.5553	-9.6553